Supporting Information

Electroless Plating NiFeP Alloy on the Surface of Silicon Photoanode for Efficient Photoelectrochemical Water Oxidation

Fusheng Li,*†[a] Yingzheng Li,†[a] Qiming Zhuo,[a] Dinghua Zhou,[a] Yilong Zhao,[a] Ziqi Zhao,[a] Xiujuan Wu,[a] Yu Shan[a] and Licheng Sun*[a, b]

a) State Key Laboratory of Fine Chemicals, Institute of Artificial Photosynthesis, DUT-KTH Joint Education and Research Centre on Molecular Devices, Institute for Energy Science and Technology, Dalian University of Technology, 116024 Dalian, China

b) Department of Chemistry, School of Engineering Sciences in Chemistry, Biotechnology and Health, KTH Royal Institute of Technology, Stockholm 10044, Sweden.

*Corresponding authors:

fusheng@dlut.edu.cn

sunlc@dlut.edu.cn

† These authors contributed equally to this work.

Materials. Single polished *n*-type silicon (P doped, 1-5 Ω cm, thickness 500 μm, <100>) and heavy doping *n*-type silicon (n^{++}-Si) (As doped, 0.001-0.0015 Ω cm) were purchased from Suzhou Crystal Silicon Electronic & Technology Co., Ltd. Nickel sulfate hexahydrate ($NiSO_4 \cdot 6H_2O$, 99%), Ferrous sulfate heptahydrate ($FeSO_4 \cdot 7H_2O$, 99%), Sodium hypophosphite (NaH_2PO_2, 99%), Ammonium fluoride (NH_4F, 99%), Trisodium citrate dihydrate ($Na_3C_6H_5O_7 \cdot 2H_2O$, 99%), Stannous chloride ($SnCl_2$, 99%), Gallium Indium eutectic (Ga-In, 99.99%), Palladium chloride ($PdCl_2$, 99%) and Potassium hydroxide (KOH, 99%) were purchased from Aladdin Reagent, China. All reagents were directly used as received without further treatment. Milli-Q water was used for the preparation of all aqueous solutions (resistance 18 MΩ cm^{-1}).

Instruments. The surface morphology of electrodes were characterized by HITACHI SU8220 field emission scanning electron microscope (FE-SEM, 5 kV), the corresponding energy dispersive X-ray (EDX) were obtained by Oxford EDS Inca Energy Coater 300 (20 kV). High-angle annular dark-field scanning transmission electron microscopy (HAADF-STEM) images and the corresponding energy-dispersive X-ray spectroscopy (EDS) mappings were collected on a FEI Talos F200X (200 kV), the samples for STEM were obtained by focus ion beam slicing (ZEISS Crossbeam 540). The surface composition of the photoanodes was investigated by X-ray photoelectron spectroscopy (XPS) on an ESCALAB Xi+ (Thermo Scientific). The pH of electrolyte was measured by 914 pH/conductometer (Metrohm). Ultraviolet–visible spectra were taken out of a solid UV-

visible spectrometer evolution 200 (Thermo Scientific).

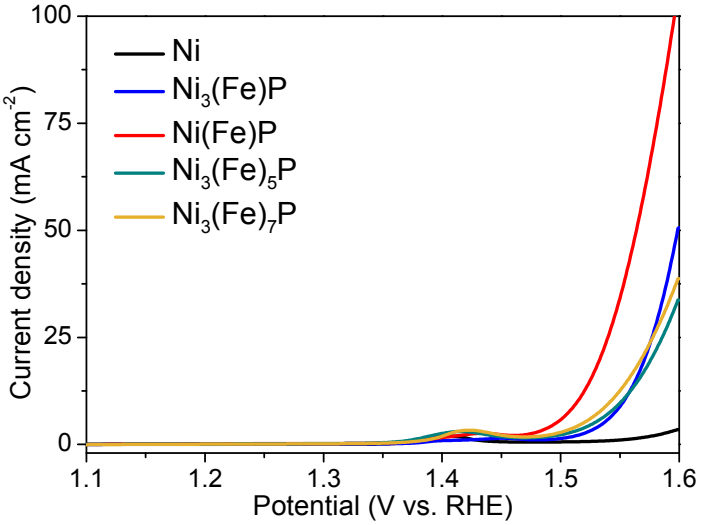

Figure S1. Polarization curves of **NiFeP/n^{++}-Si** with different proportions of Ni:Fe in the deposition solution for water oxidation, measured in 1.0 M KOH solution at a scan rate of 10 mV s^{-1}.The electrochemical test of n^{++}-Si electrode was measured by cycle voltammetry at a scan rate of 10 mV s^{-1} in 1.0 M KOH (pH=13.6) with 80% iR-compensation. All the measured potentials were converted to reversible hydrogen electrodes (RHE) according to $E_{RHE} = E_{Hg/HgO} + 0.059\ pH + 0.098$.

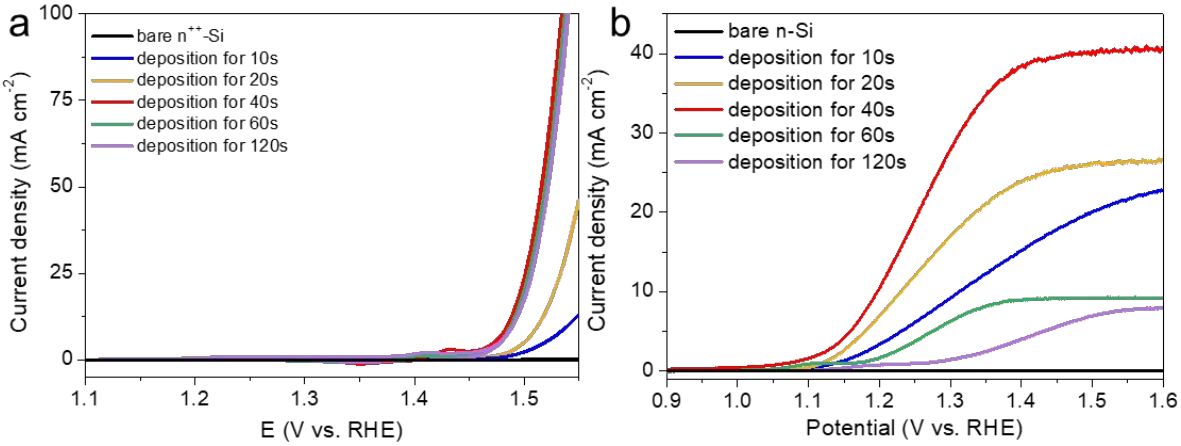

Figure S2. (a) Cyclic Voltammetry curves of **NiFeP/n^{++} Si** electrodes corresponding to different deposition times, measured in 1.0 M KOH solution at a scan rate of 10 mV s^{-1}. (b) Linear sweep voltammetry curves of **NiFeP/n-Si** photoanodes with different deposition times under irradiation, measured in 1.0 M KOH solution at a scan rate of 50 mV s^{-1}.

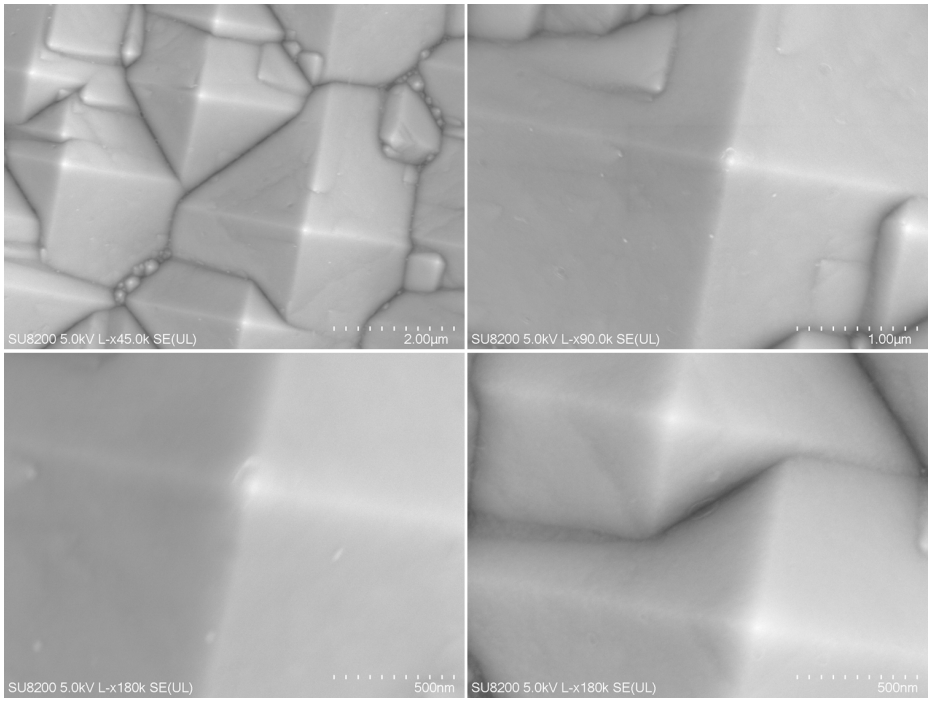

Figure S3. SEM images of the bare silicon with micro-pyramid structure at different magnification.

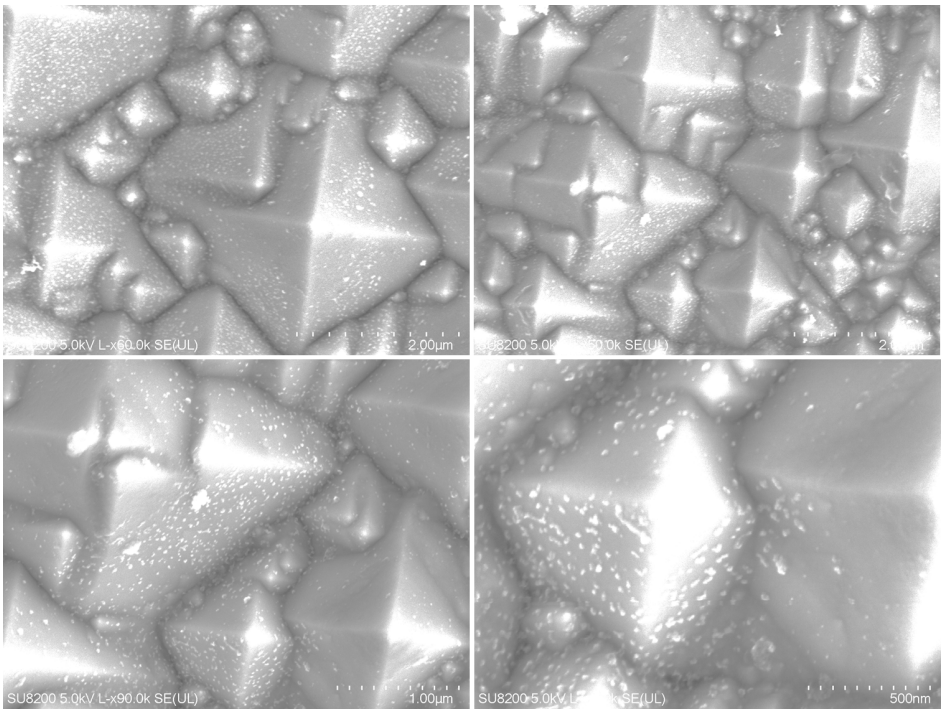

Figure S4. SEM images of the micro-pyramid structured **n-Si** treated with Sn^{2+} and Pd^{2+} (Pd^0/**n-Si**) at different magnification.

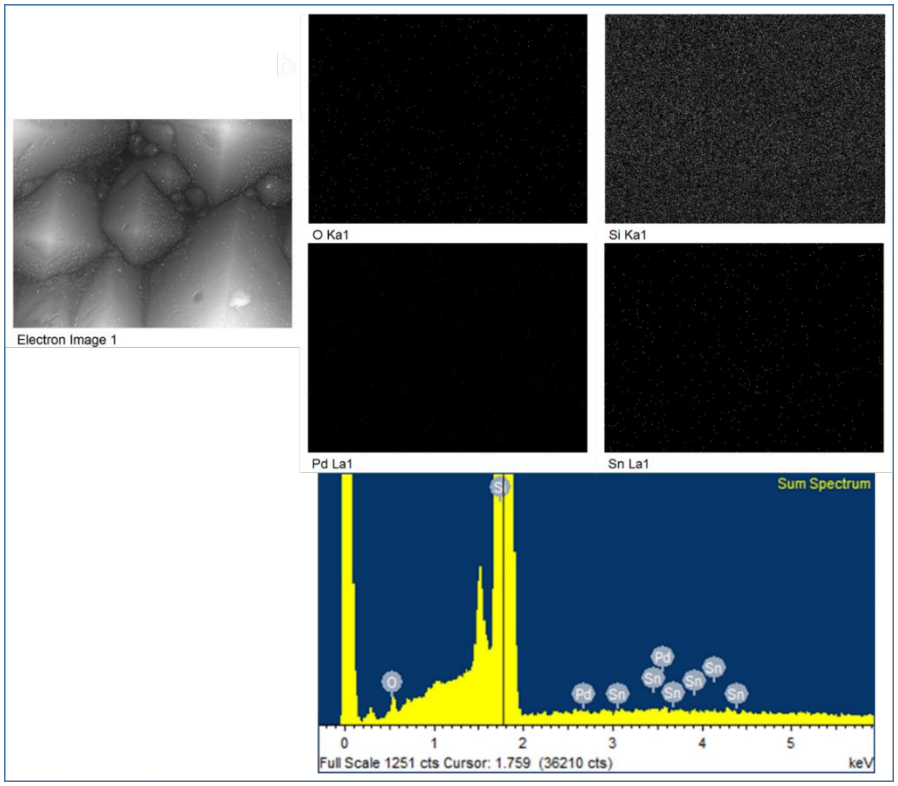

Figure S5. EDS mapping of Pd^0/**n-Si**, and the corresponding EDS spectra.

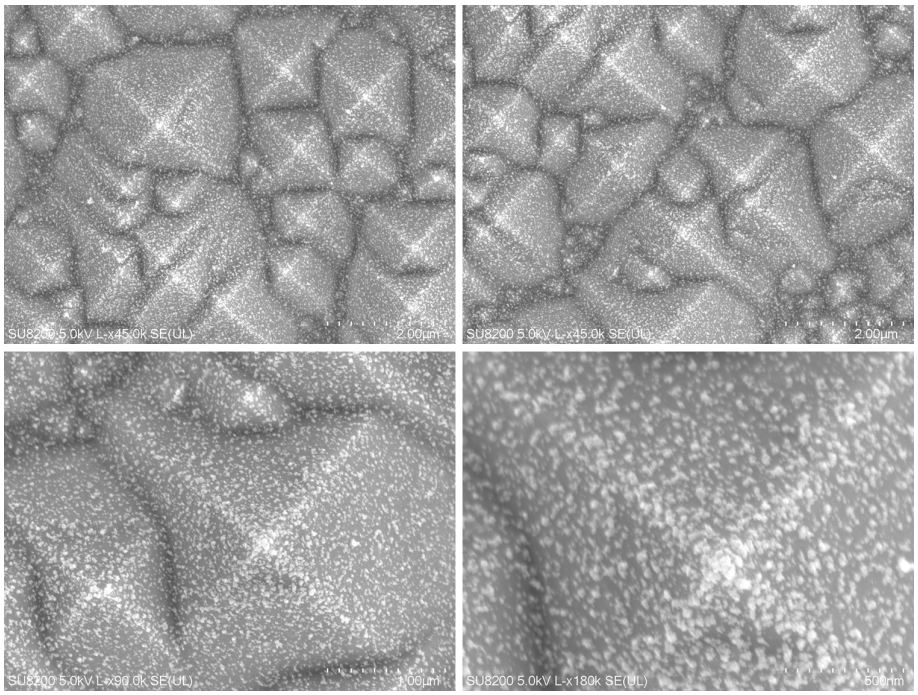

Figure S6. SEM images of **NiFeP/n-Si** electrode at different magnification prepared by electroless deposition for 10 s.

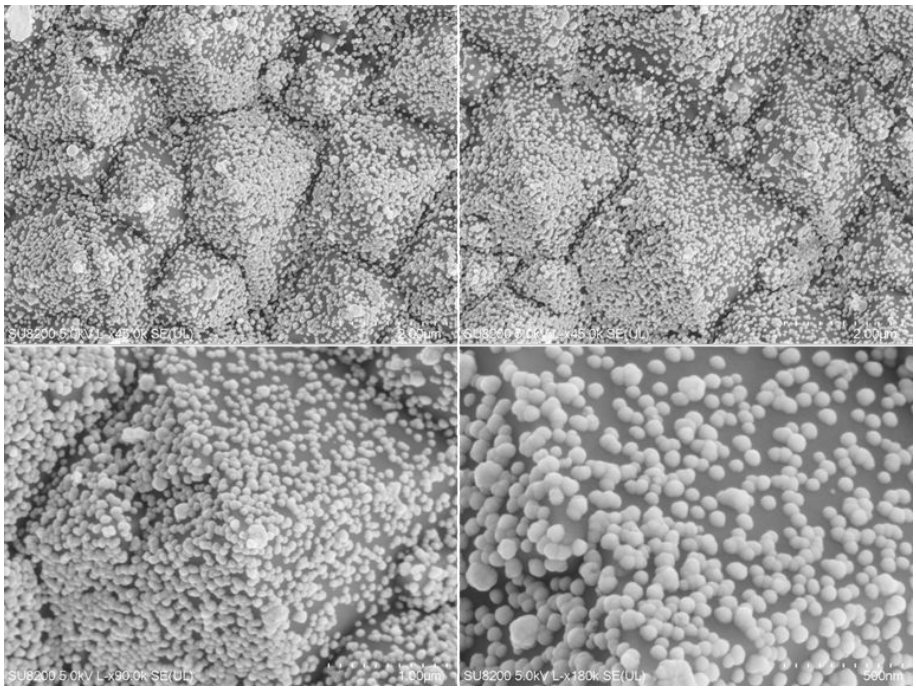

Figure S7. SEM images of **NiFeP/n-Si** electrode at different magnification prepared by electroless deposition for 20 s.

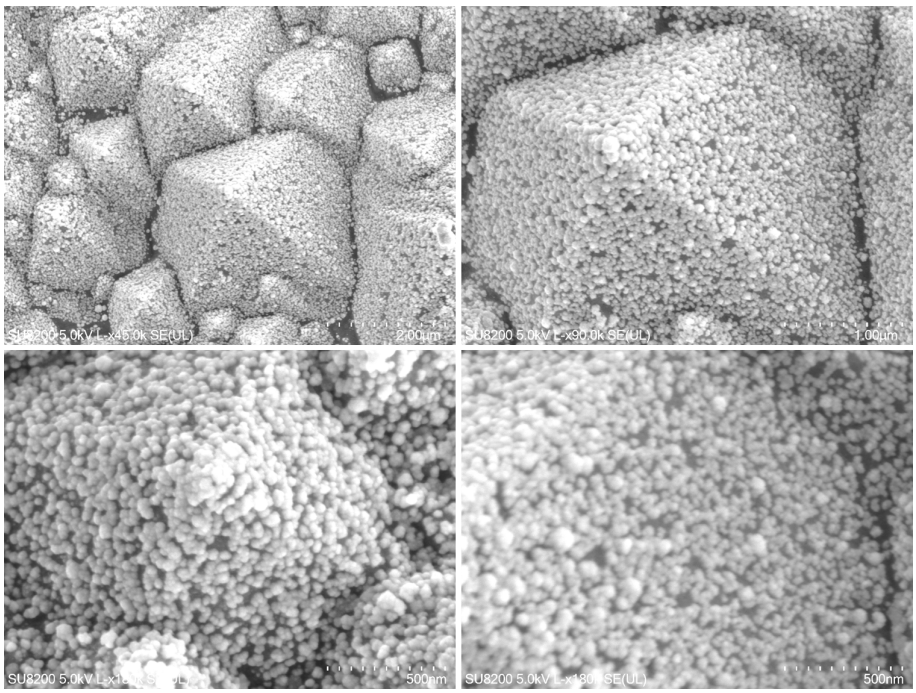

Figure S8. SEM images of **NiFeP/n-Si** electrode at different magnification prepared by electroless deposition for 40 s.

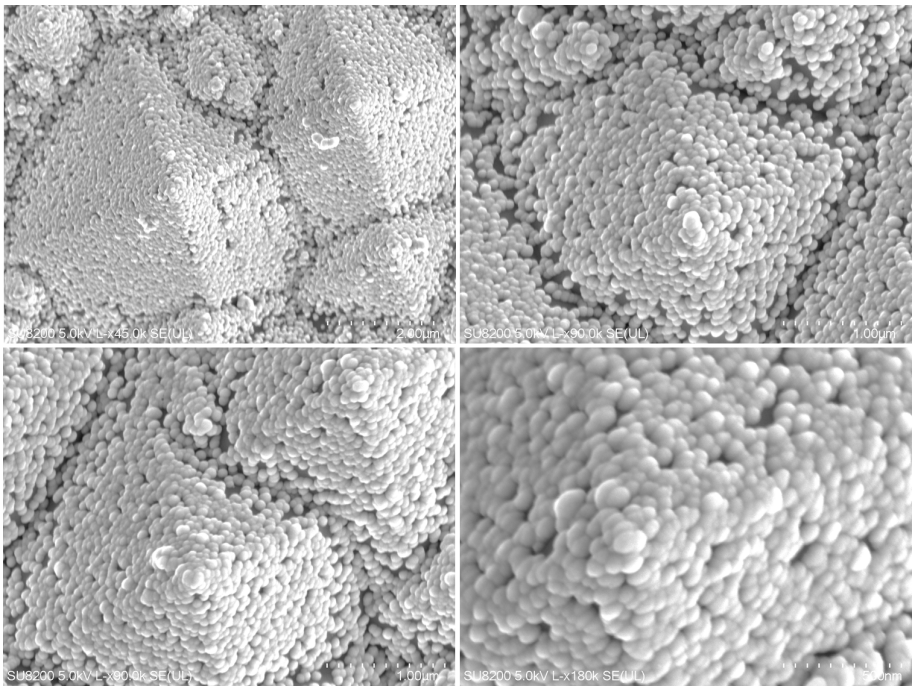

Figure S9. SEM images of **NiFeP/n-Si** electrode at different magnification prepared by electroless deposition for 60 s.

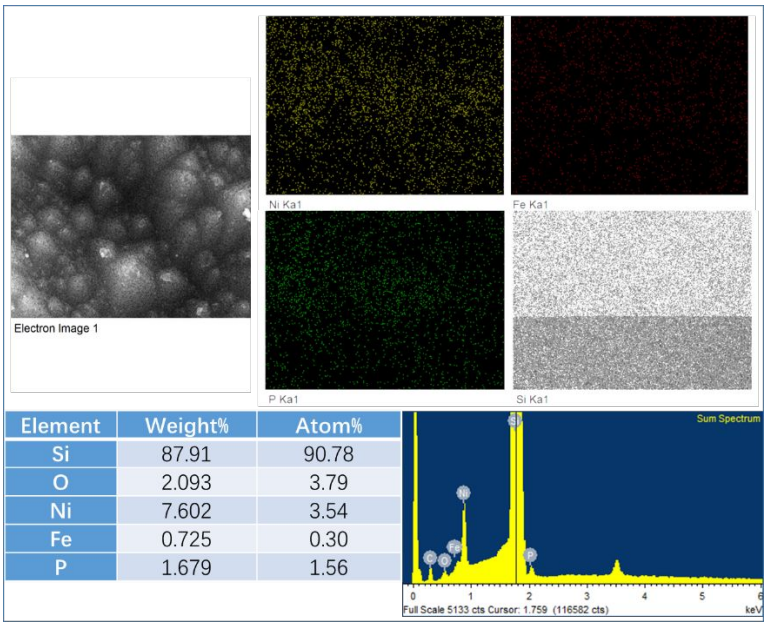

Element	Weight%	Atom%
Si	87.91	90.78
O	2.093	3.79
Ni	7.602	3.54
Fe	0.725	0.30
P	1.679	1.56

Figure S10. EDS mapping of **NiFeP/n-Si** electrode prepared by electroless deposition for 40 s, and the corresponding EDS spectra.

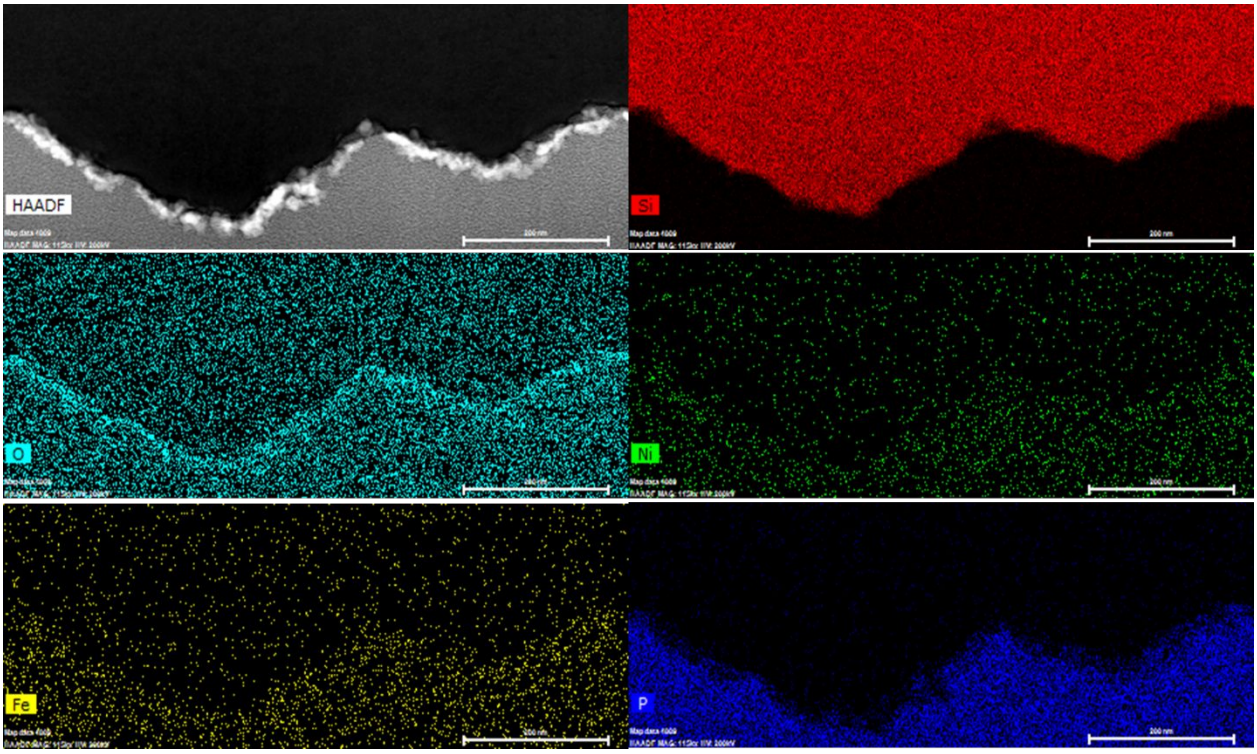

Figure S11. HAADF-STEM image and the corresponding EDS mappings of as prepared **NiFeP/n-Si** photoanode.

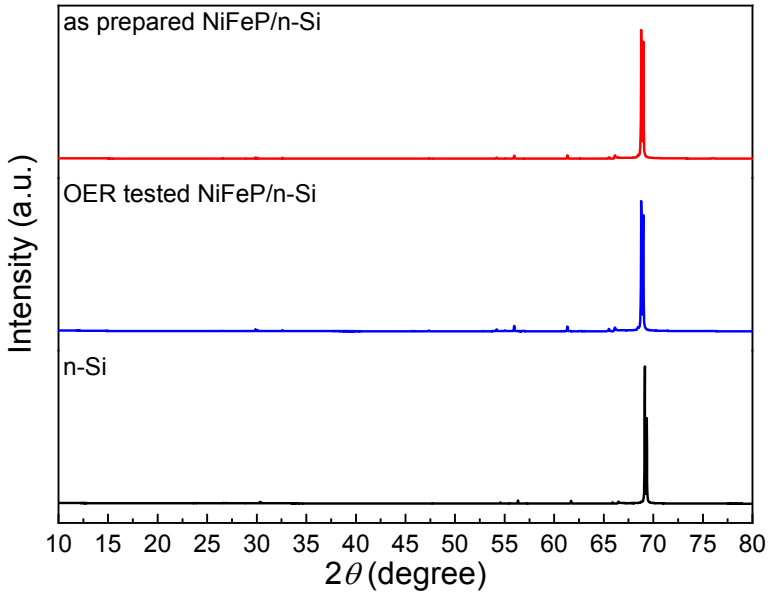

Figure S12. X-ray diffraction pattern of **n-Si**, as prepared **NiFeP/n-Si** and **NiFeP/n-Si** after 17h steady-state OER test.

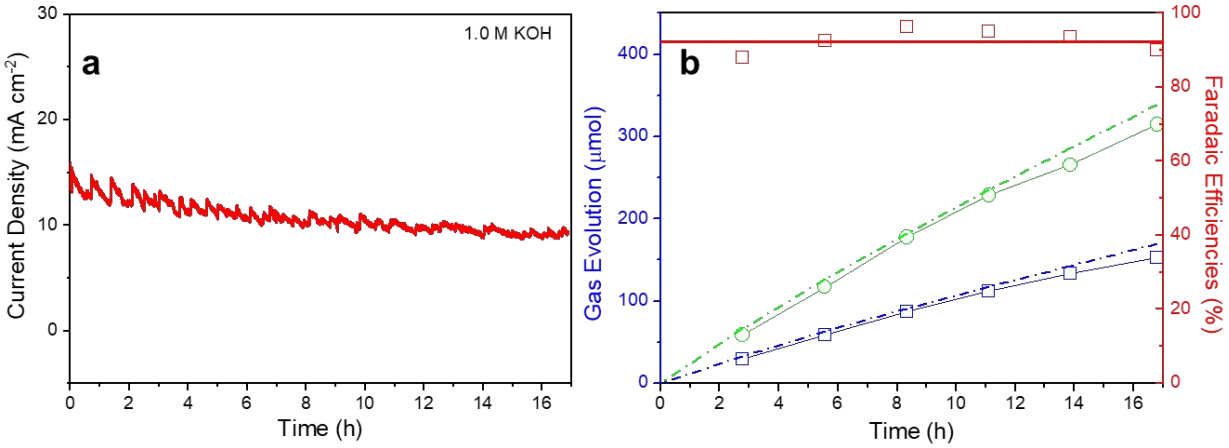

Figure S13 (a) The I-t curve corresponding to the Faradaic Efficiency measurement. (b) H_2 (green lines) and O_2 (blue lines) actual production (circles and squares) and theorical production (dot lines) vs time (h), the red squares are Faradic Efficiency corresponding to the time, and the red line is the average Faradic Efficiency.

To measure the amount of oxygen produced by the photoelectrochemical process, chronopotentiometry measurements were recorded in a sealed quartz cell (1.0 M KOH as electrolyte, **NiFeP/n-Si** as work electrode) at an applied potential of 1.23 V vs. RHE without iR compensation, the active area of the **NiFeP/n-Si** photoanode is controlled to be 0.1cm^{-2}. Before chronopotentiometry measurement, the assembled quartz cell was degassed by argon for 40 min. 0.5 mL of gas was analyzed by gas chromatography (GC, Techcomp GC 7890T, Ar as the carrier gas, Thermo Conductivity Detector).

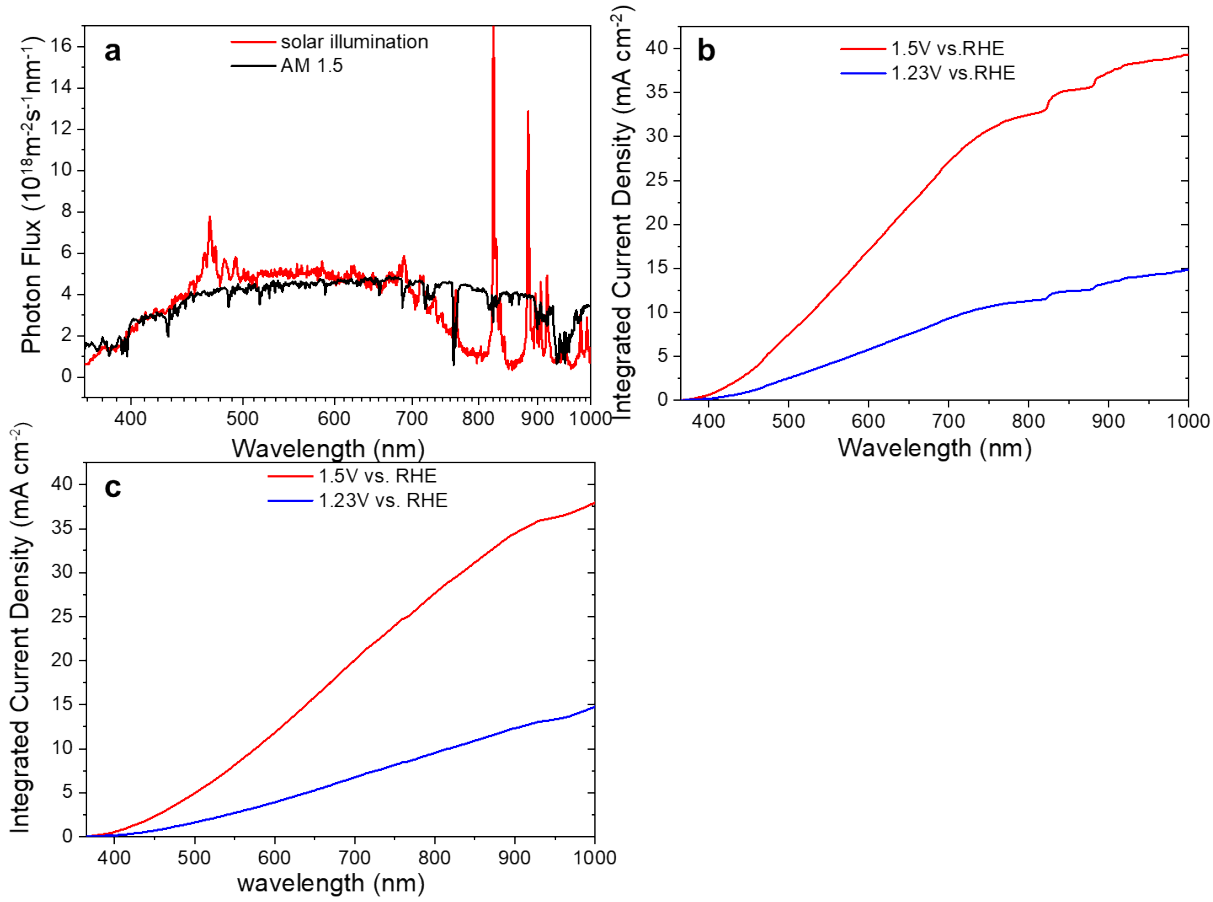

Figure S14. (a) Irradiance spectra of the ASTM G173-03 (AM1.5G) and the solar simulator with AM 1.5G filter. (b) The calculated photocurrents of **NiFeP/n-Si** by integrating IPCE at 1.23V and 1.5V vs. RHE over the photon flux of solar illuminator. (c) The calculated photocurrents of **NiFeP/n-Si** by integrating IPCE at 1.23V and 1.5V vs. RHE over the photon flux of ASTM G173-03.

Table S1. **PEC performance of recently published silicon photoanodes with Ni based catalyst.**

Photoanode Structure	Fabrication Methods	Electrolyte	Current density @1.23V vs. RHE (mA cm^{-2})	Saturation Current density (mA cm^{-2})	Stability (h)	Ref.
NiFeP/n-Si	**ELD**	**1.0 M KOH**	**15.5**	**40.5**	**17**	**This work**
NiFeP/n-Si	**ELD**	**1.0 M KBi**	**2.3**	**38**	**75**	**This work**
Ni/SiO_2/n-Si	ELD+ photolithography	1.0 M KOH	7	27.5	24	1
NiFe NP/black n-Si	ED	1.0 M KOH	4.3	23.8	16	2
Ni/n-Si	ED	1.0 M KOH	3.5	32.5	10	3
NiFe/np^+Si	ED	1.0 M KOH	30	30	12	4
$NiSe_2$/n-Si	CVD+calcination	1.0 M KOH	5	8	2	5
Ni-Au/n-Si	TE+ED	1.0 M KBi	0	30	null	6
NiFe NPs/n-Si	TE	1.0 M KOH	25.2	30	22.5	7
NiO_x/Graphdiyne Nanowall/ITO/ n^+np^+-Si	MS+chemical liquid deposition	1.0 M KOH	<5	39.1	null	8
NiOOH/ITO/TiO_2/n-Si	ALD+ MS+ED	1.0 M LiOH	18	40	null	9
$Co(OH)_2$/TiO2/b-Si	ALD+ED	1.0 M KOH	2	32	4	10
$NiMoO_4$/TiO_2/n-Si	ALD+ Hydrothermal	0.25 M KOH	0	20	0.2	11
NiOOH/NiO/Ni/ Al_2O_3/SiO_2/Si	ALD+ MS	1.0 M KOH	28	30	80	12
CoO_x/n-Si	ALD	1.0 M KOH	20	30	2500	13
CoO_x/TiO_2/n-Si	ALD	1.0 M KOH	3.5	32.5	12	14
$NiCuO_x$/CoO_x/n-Si	ALD+spin-coating	1.0 M KOH	15	28.3	22.6	15
NiAu NPs/TiO_2/n-Si	ALD+e-beam	1.0 M KOH	18.8	35	20	16
Ni/TiO_2/np^+Si	ALD+e-beam	1.0 M KOH	10	35	100	17
Ni Ni-Mo/n^+np^+-Si	e-beam	1.0 M KOH	32	37	100	18
Ni/n-Si	e-beam	1.0 M KOH	10 (2 sun)	57 (2 sun)	80	19

ELD = Electroless deposition, Electrodeposition = ED, Thermal evaporation = TE, Magnetron sputtering = MS, Atomic layer deposition = ALD, Chemical vapor deposition = CVD, Electron Beam Evaporation = e-beam

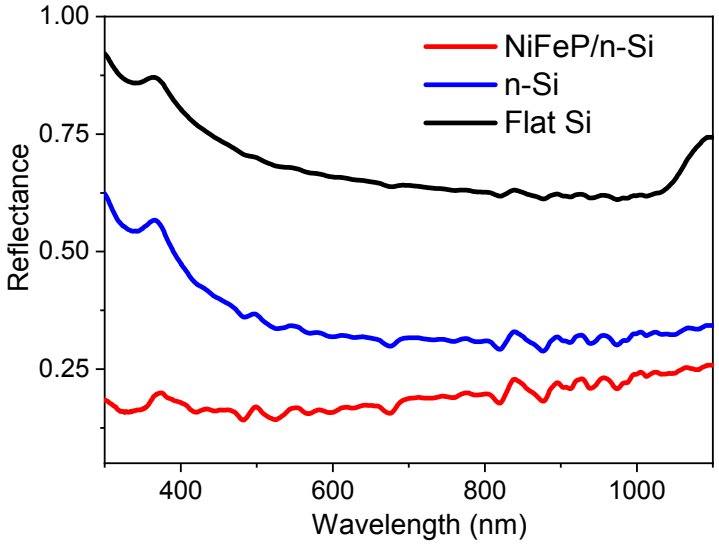

Figure S15. Reflectance spectra of **NiFeP/n-Si**, micro-pyramid silicon (**n-Si**) and flat silicon measured by UV visible diffuse reflectance spectrometer.

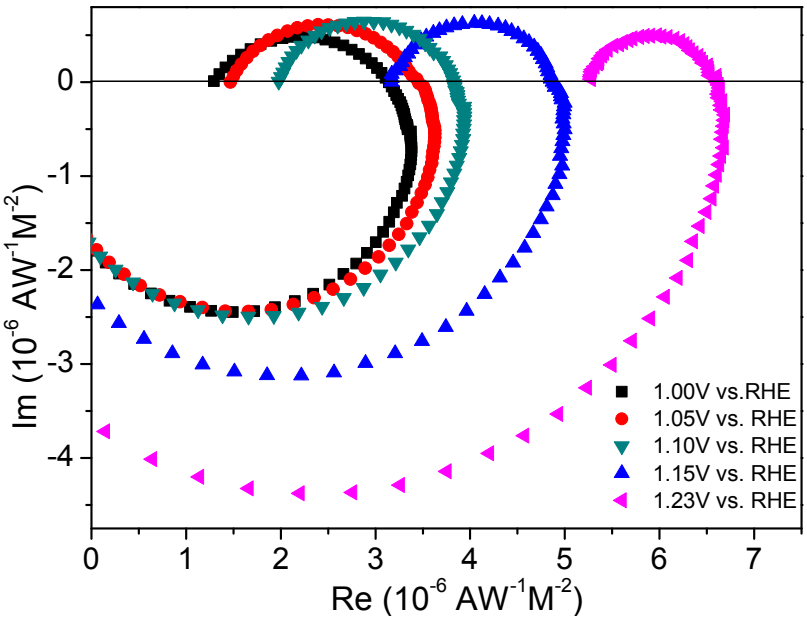

Figure S16. IMPS curves of **NiFeP/n-Si** electrodes measured in 1.0 M KOH at bias potential of 0.33 V vs. Hg/HgO (1.23 V vs.RHE).

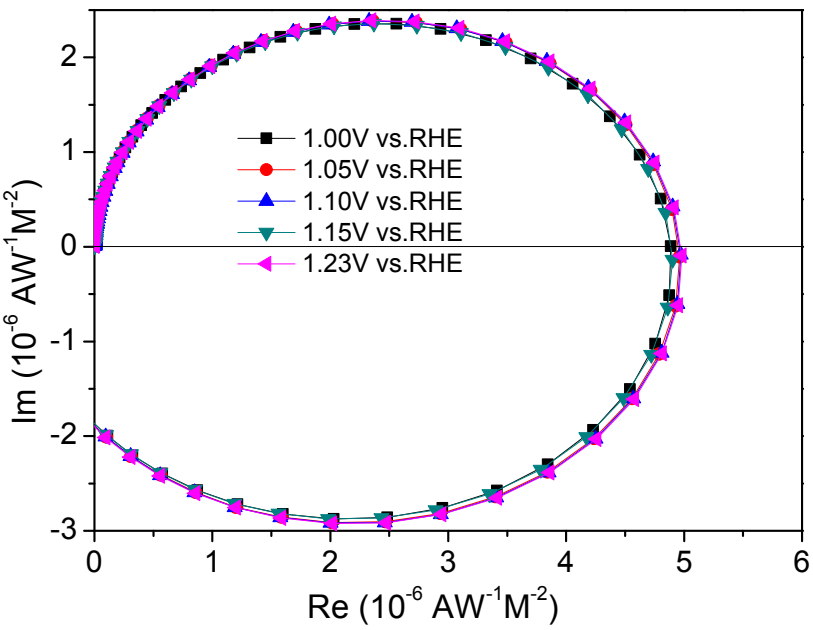

Figure S17. IMPS of **n-Si** electrodes measured in 1.0 M KOH at bias potential of 0.33 V vs. Hg/HgO (1.23 V vs.RHE).

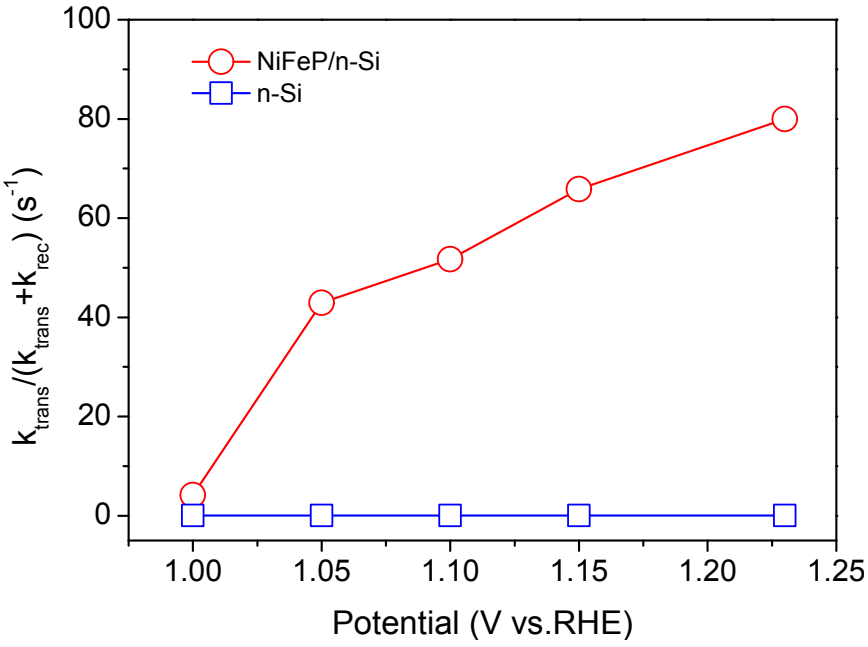

Figure S18.Charge transfer efficiency of **NiFeP/n-Si** at 1.23V vs. RHE calculated by IMPS spectra.

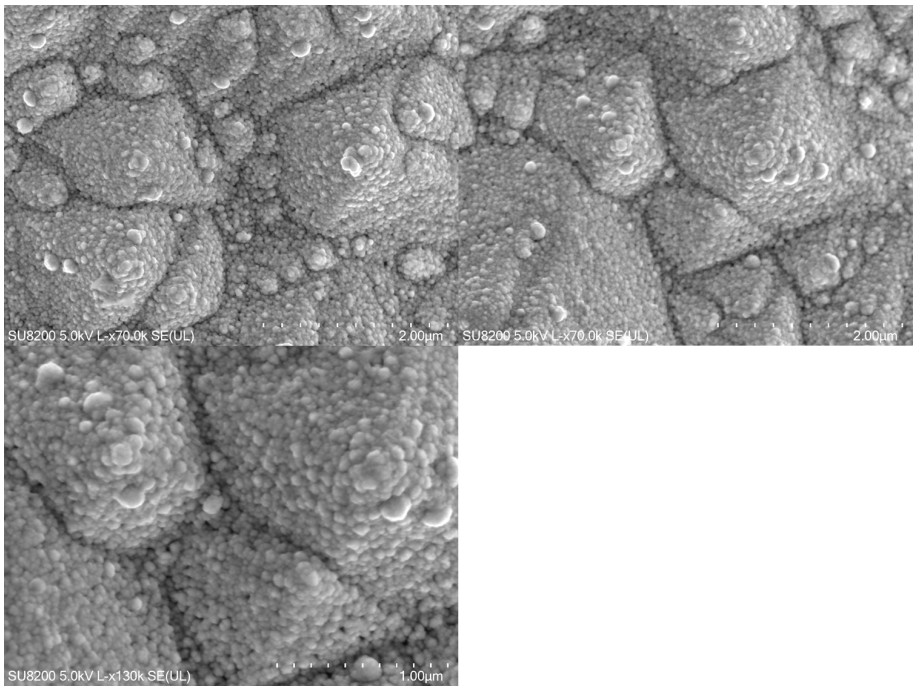

Figure S19. SEM images of **NiFeP/n-Si** electrode 17 h continuous PEC measurement in 1.0 M KOH solution at 1.23 V vs RHE.

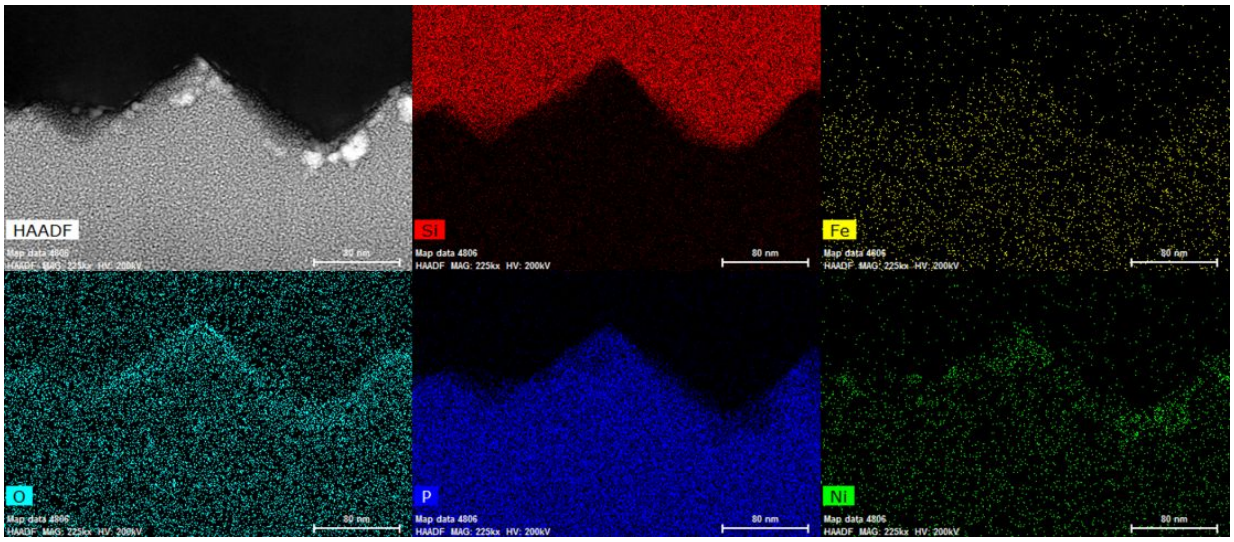

Figure S20. HAADF-STEM images and corresponding EDS mappings of **NiFeP/n-Si** photoanodes after steady-state OER test.

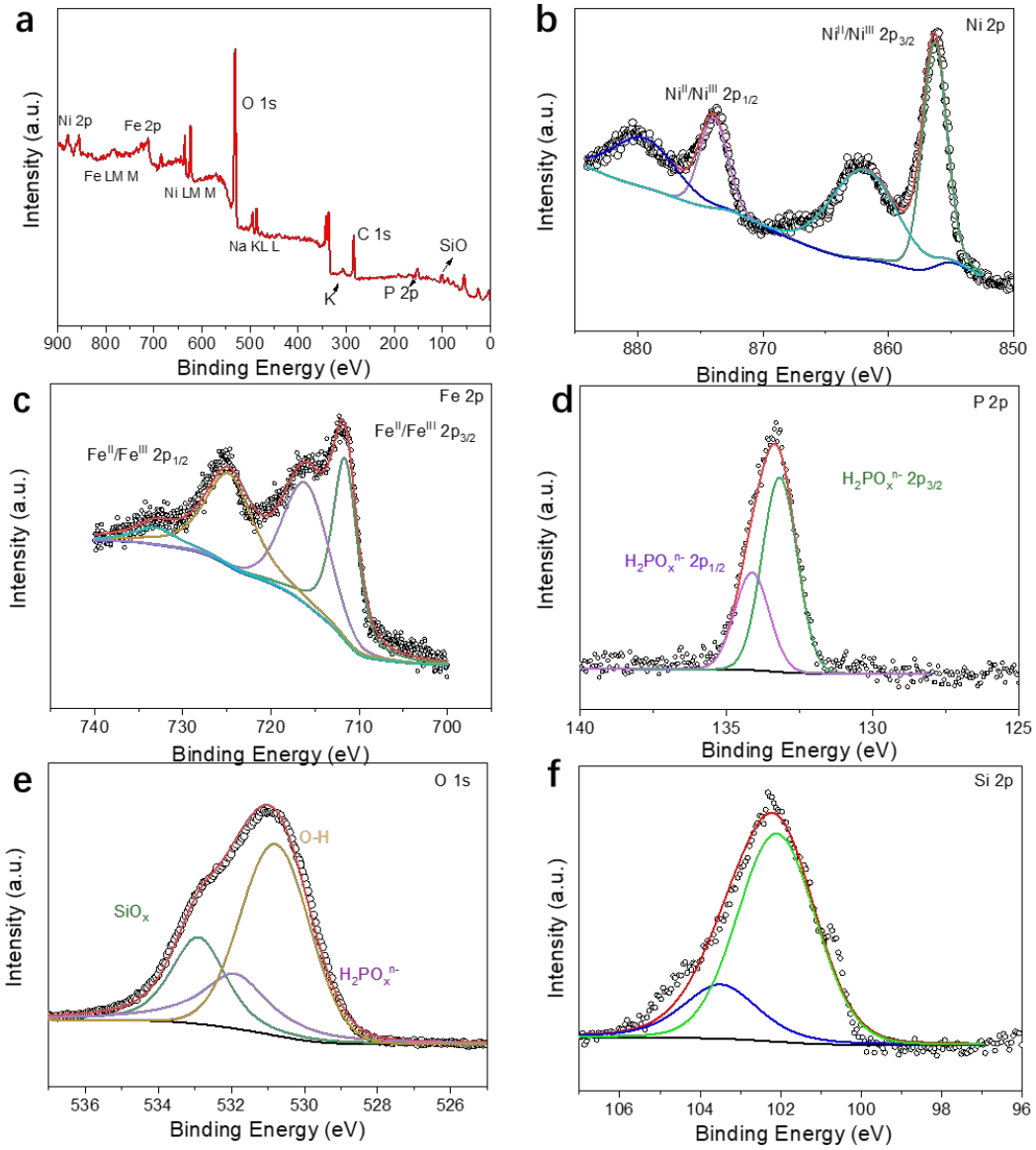

Figure S21. (a) XPS data of **NiFeP/n-Si** after 17h OER tested; High-resolution XPS spectra of (b) Ni 2p (c) Fe 2p (d) P 2p (e) O1s and (f) Si 2p for **NiFeP/n-Si** after 17h steady-state OER test. The scatter line is the raw data and the red line is the fitting result.

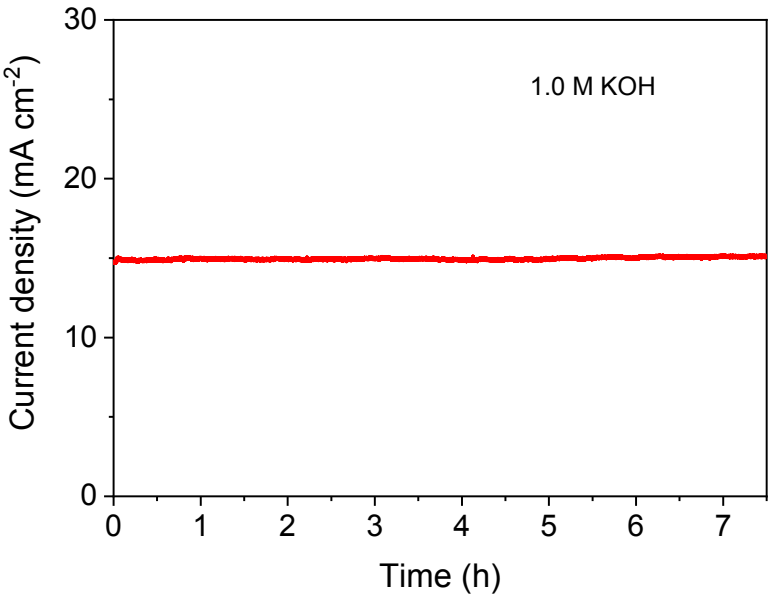

Figure S22. I–t curve of **NiFeP(60s)/n^{++}-Si** photoanode under light irradiation at a constant bias of 1.55 V vs. RHE with 1.0 M KOH as the electrolyte without iR compensation.

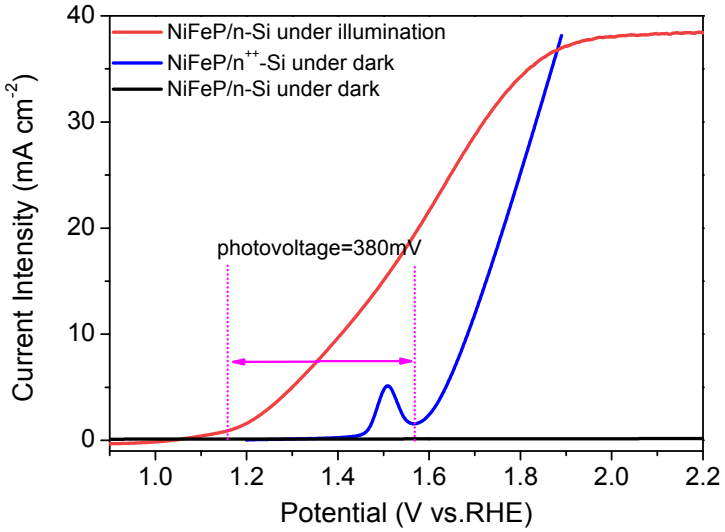

Figure S23. J–V curves of **NiFeP/n-Si** photoanode under AM 1.5G simulated sunlight at 100 mW cm^{-2} and the electrocatalytic activity of **NiFeP/n^{++}-Si** electrode measured in 1.0 M KOH with 1.0 M H_3BO_3 (1M K-borate, pH=9.2) with a scan rate of 50 mV s^{-1} and 10 mV s^{-1}.

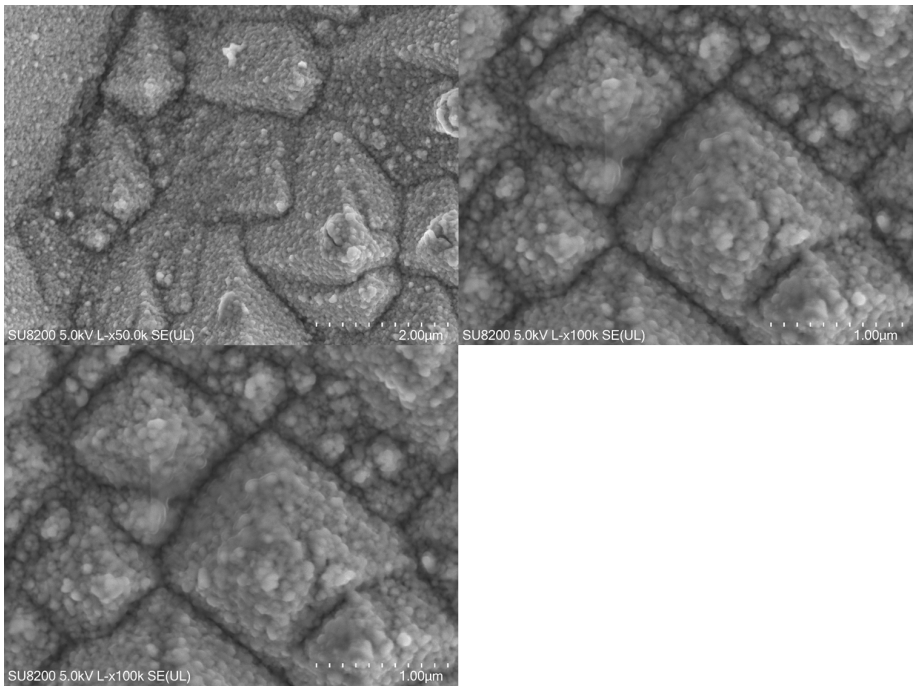

Figure S24. SEM images of **NiFeP(40s)/n-Si** electrode after 75 h continuous PEC measurement in 1.0 M KBi solution.

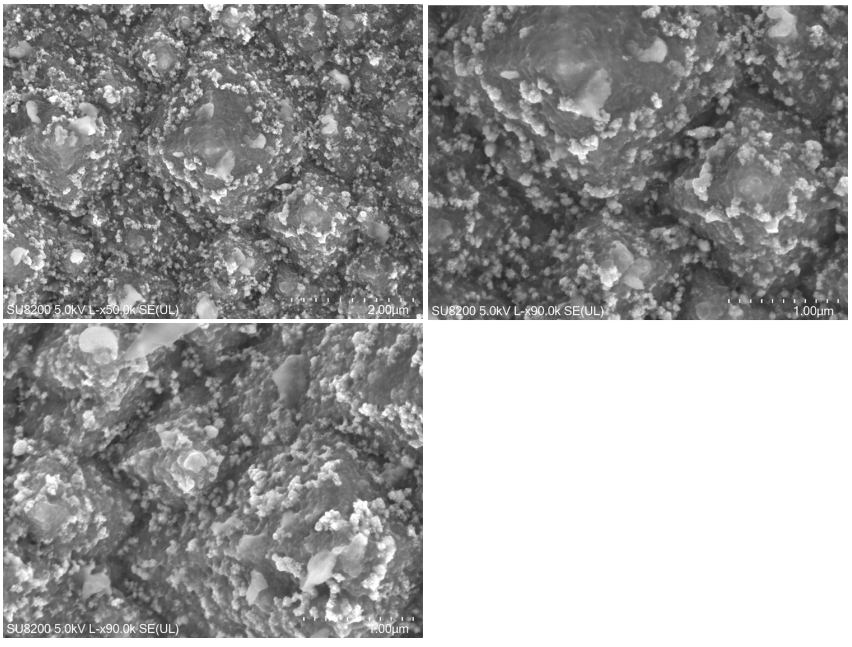

Figure S25. SEM images of **NiFeP**(20s)**/n-Si** electrode after 90 min continuous PEC measurement in 1.0 M KOH solution.

Supplementary note:

The proposed reaction mechanisms of NiFeP electroless deposition on n-Si, the activation process can be described by the reactions given below:

$$Sn^{2+}+Pd^{2+} \longrightarrow Sn^{4+}+Pd^{0}$$

At first, the Sn^{2+} is absorbed to the surface of silicon in the activation solution A, and then, the Pd^0 produced on the surface of n-Si in the solution B by the reaction given above which results as the catalyst of the beginning of the deposition process. At the beginning of the electroless deposition, the deposition reaction is catalyzed by the Pd^0, as the NiFeP alloy depositing, the deposition reaction can be catalyzed by the Ni^0 and Fe^0 and the reaction rate increased with the amount of NiFeP alloy increasing.[20-23]

$$H_2PO_2^- + H_2O \longrightarrow H_2PO_3^{2-} + 2H^+ + 2e^-$$

$$H_2PO_2^- + 2H^+ + e^- \longrightarrow P + 2H_2O$$

$$Ni^{2+}(Fe^{2+}) + e^- \longrightarrow Ni_{ads}^{1}\,(Fe_{ads}^{1})$$

$$Ni_{ads}^{1}(Fe_{ads}^{1}) + e^- \longrightarrow Ni\,(Fe)$$

$$2H^+ + 2e^- \longrightarrow H_2$$

Supplementary Reference

(1) Zhao, J.; Gill, T. M.; Zheng, X., Enabling Silicon Photoanodes for Efficient Solar Water Splitting by Electroless-deposited Nickel. *Nano Res.* **2018**, *11*, 3499.

(2) Oh, K.; Joanny, L.; Gouttefangeas, F.; Fabre, B.; Dorcet, V.; Lassalle-Kaiser, B.; Vacher, A.; Mériadec, C.; Ababou-Girard, S.; Loget, G., Black Silicon Photoanodes Entirely Prepared with Abundant Materials by Low-Cost Wet Methods. *ACS Applied Energy Materials* **2019**, *2*, 1006.

(3) Loget, G.; Fabre, B.; Fryars, S.; Mériadec, C.; Ababou-Girard, S., Dispersed Ni Nanoparticles Stabilize Silicon Photoanodes for Efficient and Inexpensive Sunlight-Assisted Water Oxidation. *ACS Energy Lett.* **2017**, *2*, 569.

(4) Yu, X.; Yang, P.; Chen, S.; Zhang, M.; Shi, G., NiFe Alloy Protected Silicon Photoanode for Efficient Water Splitting. *Adv. Energy Mater.* **2017**, *7*, 1601805.

(5) Lee, S.; Cha, S.; Myung, Y.; Park, K.; Kwak, I. H.; Kwon, I. S.; Seo, J.; Lim, S. A.; Cha, E. H.; Park, J., Orthorhombic NiSe2 Nanocrystals on Si Nanowires for Efficient Photoelectrochemical Water Splitting. *ACS Appl. Mater. Interfaces* **2018**, *10*, 33198.

(6) Laskowski, F. A. L.; Nellist, M. R.; Venkatkarthick, R.; Boettcher, S. W., Junction Behavior of n-Si Photoanodes Protected by Thin Ni Elucidated from Dual Working Electrode Photoelectrochemistry. *Energy Environ. Sci.* **2017**, *10*, 570.

(7) Li, C.; Huang, M.; Zhong, Y.; Zhang, L.; Xiao, Y.; Zhu, H., Highly Efficient NiFe Nanoparticle Decorated Si Photoanode for Photoelectrochemical Water Oxidation. *Chem. Mater.* **2018**, *31*, 171.
(8) Zhang, S.; Yin, C.; Kang, Z.; Wu, P.; Wu, J.; Zhang, Z.; Liao, Q.; Zhang, J.; Zhang, Y., Graphdiyne Nanowall for Enhanced Photoelectrochemical Performance of Si Heterojunction Photoanode. *ACS Appl Mater Interfaces* **2019**, *11*, 2745.
(9) Yao, T.; Chen, R.; Li, J.; Han, J.; Qin, W.; Wang, H.; Shi, J.; Fan, F.; Li, C., Manipulating the Interfacial Energetics of n-type Silicon Photoanode for Efficient Water Oxidation. *J. Am. Chem. Soc.* **2016**, *138*, 13664.
(10) Yu, Y.; Zhang, Z.; Yin, X.; Kvit, A.; Liao, Q.; Kang, Z.; Yan, X.; Zhang, Y.; Wang, X., Enhanced Photoelectrochemical Efficiency and Stability Using a Conformal TiO_2 Film on a Black Silicon Photoanode. *Nat. Energy* **2017**, *2*, 17045.
(11) Wu, F.; Liao, Q.; Cao, F.; Li, L.; Zhang, Y., Non-noble Bimetallic $NiMoO_4$ Nanosheets Integrated Si Photoanodes for Highly Efficient and Stable Solar Water Splitting. *Nano Energy* **2017**, *34*, 8.
(12) Luo, Z.; Liu, B.; Li, H.; Chang, X.; Zhu, W.; Wang, T.; Gong, J., Multifunctional Nickel Film Protected n-Type Silicon Photoanode with High Photovoltage for Efficient and Stable Oxygen Evolution Reaction. *Small Methods* **2019**, *3*, 1900212.
(13) Zhou, X.; Liu, R.; Sun, K.; Papadantonakis, K. M.; Brunschwig, B. S.; Lewis, N. S., 570 mV Photovoltage, Stabilized n-Si/CoO_x Heterojunction Photoanodes Fabricated Using Atomic Layer Deposition. *Energy Environ. Sci.* **2016**, *9*, 892.
(14) Oh, S.; Jung, S.; Lee, Y. H.; Song, J. T.; Kim, T. H.; Nandi, D. K.; Kim, S.-H.; Oh, J., Hole-Selective CoO_x/SiO_x/Si Heterojunctions for Photoelectrochemical Water Splitting. *ACS Cata.* **2018**, *8*, 9755.
(15) He, L.; Zhou, W.; Hong, L.; Wei, D.; Wang, G.; Shi, X.; Shen, S., Cascading Interfaces Enable n-Si Photoanodes for Efficient and Stable Solar Water Oxidation. *J Phys. Chem. Lett.* **2019**, *10*, 2278.
(16) Hong, W.; Cai, Q.; Ban, R.; He, X.; Jian, C.; Li, J.; Li, J.; Liu, W., High-Performance Silicon Photoanode Enhanced by Gold Nanoparticles for Efficient Water Oxidation. *ACS Appl Mater Interfaces* **2018**, *10*, 6262.
(17) Hu, S.; Shaner, M. R.; Beardslee, J. A.; Lichterman, M.; Brunschwig, B. S.; Lewis, N. S., Amorphous TiO_2 Coatings Stabilize Si, GaAs, and GaP Photoanodes for Efficient Water Oxidation. *Science* **2014**, *344*, 1005.
(18) Fan, R.; Cheng, S.; Huang, G.; Wang, Y.; Zhang, Y.; Vanka, S.; Botton, G. A.; Mi, Z.; Shen, M., Unassisted Solar Water Splitting with 9.8% Efficiency and Over 100 h Stability Based on Si Solar Cells and Photoelectrodes Catalyzed by Bifunctional Ni–Mo/Ni. *J. Mater. Chem. A* **2019**, *7*, 2200.
(19) Kenney, M. J.; Gong, M.; Li, Y.; Wu, J. Z.; Feng, J.; Lanza, M.; Dai, H., High-Performance Silicon Photoanodes Passivated with Ultrathin Nickel Films for Water Oxidation. *Science* **2013**, *342*, 836.
(20) Yang, W.; Fu, Y.; Xia, A.; Zhang, K.; Wu, Z., Microwave Absorption Property of Ni–Co–Fe–P-coated Flake Graphite Prepared by Electroless Plating. *J. Alloys Compd.* **2012**, *518*, 6.
(21) Aal, A. A.; Shaaban, A.; Hamid, Z. A., Nanocrystalline Soft Ferromagnetic Ni–Co–P Thin Film on Al alloy by Low Temperature Electroless Deposition. *Appl. Surf. Sci.* **2008**, *254*, 1966.
(22) Dubin, V. M., Electroless Ni-P Deposition on Silicon with Pd Activation. *J. Electrochem. Soc.* **1992**, *139*, 1289.
(23) Tsai, T.-K.; Chao, C.-G., The Growth Morphology and Crystallinity of Electroless NiP Deposition on Silicon. *Appl. Surf. Sci.* **2004**, *233*, 180.